



Combined Hill-Taylor Theory: Theoretical, Experimental and Finite Element Study

Faraz Rahimzadeh Lotfabad, Ramin Ebrahimi*

Department of Materials Science and Engineering, School of Engineering, Shiraz University, Shiraz, Iran.

Received: 13 July 2021; Accepted: 11 September 2021

*Corresponding author email: ebrahimi@shirazu.ac.ir

ABSTRACT

In this study, by combining crystal plasticity notions developed by Taylor and the mathematical expression of Hill's yield criterion for anisotropic materials, a model is introduced to describe the flow behavior of grains in a grain aggregate. In this model, Hill's yield criterion coefficients are calculated in terms of Taylor factors for different straining conditions for each grain. The convexity of the proposed model is proved by sign determination of the eigenvalues of the associated Hessian matrix. It is found that the experimental load-displacement curves of specimens showing the size effect are enveloped by the bounds obtained from simulations using the proposed model, which to some extent verifies the applicability of the developed model. Using the developed model, the microforging of miniature rods consisting of 50 and 200 grains in their cross-section are simulated. In agreement with the literature, the results showed that due to the difference in the mechanical behavior of grains, the distribution of strain abruptly changes from one grain to another. Moreover, it is shown that as the number of grains in the cross-section of the specimen increases, the plastic equivalent strain tends toward that predicted by the classical plasticity theories, proving the applicability of the proposed model. Finally, the results suggest that the successful production of microparts by forming processes requires raw materials in microforming to be the products of the severe plastic deformation techniques, where the microstructure is scaled down to the nanometer.

Keywords: Hill's yield criterion; Meso-scale modeling; Microforming; Size Effect, Taylor factor; Finite Element Analysis

1. Introduction

Each phenomenon can be studied at different length scales, namely macro-scale, meso-scale and micro-scale. Consider the plastic deformation of crystalline material. This phenomenon can be macro-modeled with the simple form of the following criterion: $f(\sigma_{ij})=Y$, which means that the plastic deformation occurs as a combination of stresses acting on a point reaches a specific value such as Y . The problem now is to find the best f that fits the experimental data. On the other hand, the phenomenon of plastic deformation can be micro-modeled by considering the dislocations, the

interactions of the dislocations with each other, the crystal defects, etc. This type of modeling requires sophisticated mathematical models and numerical procedures.

Despite their simplicity, some phenomena cannot be captured by macro-scale models, such as the size effect phenomenon. As the size of the regions in material, where the local mechanical behavior is different from the overall mechanical behavior, increases and becomes comparable with the dimensions of the specimen, classical plasticity rules cannot be used to analyze the process. In this case, analyzing the deformation of the material

requires models studying the plasticity of a grain aggregate in more detail. The meso-scale models are relatively simpler tools than micro-scale models, where they are able to explain some range of phenomena such as the size effect. Traces of the meso-scale modeling of the plasticity of crystalline materials can be found in the works of Schmid & Boas [1], Sachs [2], Cox & Sopwith [3], Taylor [4,5], Taylor & Elam [6], and Bishop & Hill [7]. Schmid proposed that the deformation in crystals would occur by the relative motion of certain crystal planes in specific directions (slip). According to Schmid, when stress is imposed on a single crystal, the first combination of the plane and direction on that plane, the resolved shear stress on which is reached to the critical value of τ_{CRSS} would be responsible for the plastic deformation. Sachs, and Cox & Sopwith applied the Schmid law to the plastic deformation of a crystal aggregate and assumed that each grain in a crystal aggregate would deform by the slip on a slip system with the highest shear stress acting on that. Later, Taylor's studies showed that slip in a crystal aggregate differs from the slip in single crystals concerning the degree of freedom. Once a single crystal is stressed, only one strain component is predetermined; the strain in the applied stress direction. The rest of the strain components would be determined based on the activated slip system(s). On the other hand, as the crystal aggregate is stressed, all strain components are predetermined. Hence, at least five slip systems in a crystal must be activated for a crystal aggregate to undergo an arbitrary shape change in such circumstances.

Size effect may be approached by several strategies concerning meso-scale models of plasticity such as strain gradient plasticity [8-10], mixture models [11-14], statistical-based models [15-17]. The present study aims to develop a simple framework to simulate the deformation of grains in an aggregate and study the plasticity of miniature specimens, which have a long history in the literature [18-25]. The developed model is operable in many commercial finite element codes, without the requirement of any further coding. In this study, first, a model for the plastic behavior of grains in a crystal aggregate is achieved by combining the crystal plasticity notions developed by Taylor and the mathematical form of Hill's yield criterion. Hill's yield criterion was previously employed to study the near crack tip plasticity of superalloy single-crystals applied in turbine

blades [26], where the coefficients of Hill's yield criterion were obtained by the Schmid factor. Here, as a result of the difference between plastic deformation of a single crystal alone with grain in an aggregate, coefficients of Hill's yield criterion are related to Taylor factors for different states of strain. This developed model is then studied to meet the criterion of being convex. Using this model, the microforging of miniature rods into prismatic pieces with equilateral triangle cross-sections for an isotropic specimen, a specimen composed of 50 grains and a specimen composed of 200 grains, are simulated. To evaluate the validity of the model, the extreme bounds of the force-displacement curve for the prescribed microforging process are obtained and compared with the experimental tests.

2. Materials and Methods

2.1. Combined Hill-Taylor Model

Taylor factor is defined as [27]:

$$\bar{\sigma} = M \tau_{CRSS} \quad (1)$$

Where $\bar{\sigma}$ is the effective stress, M is the Taylor factor, and τ_{CRSS} is the critical resolved shear stress. The value of M depends on the orientation of the grain and the global state of strain. For example, consider a grain oriented with Euler angles $(\varphi_1, \Phi, \varphi_2) = (54^\circ, 71.4^\circ, 186.7^\circ)$ with respect to the global frame xyz . If the specimen is stressed along the x -axis, the imposed strain condition would be $[E] = \text{diag}[1, -0.5, -0.5]$, then the Taylor factor for that grain would be 3.1373, and based on Eq. (1), the strength of that grain would be $\bar{\sigma} = 3.137 \tau_{CRSS}$ (procedure of calculation of Taylor factor is described in appendix A.1). Now, if the specimen is stressed along the y -axis, the state of strain would be $[E] = \text{diag}[-0.5, 1, -0.5]$. In this situation, the Taylor factor of that grain would be 2.5442, and based on Eq. (1), the strength of that grain would be $\bar{\sigma} = 2.5442 \tau_{CRSS}$. This example demonstrates that the well-known anisotropic mechanical behavior of the grains in an aggregate can be explained by the Taylor factor. This is used in [28-30] to justify loading direction dependency and orientation dependency of mechanical behavior of materials.

Hill's yield criterion [31] with the form of Eq. (2) is capable of describing anisotropic mechanical behavior. However, it is better to carefully be stated that only the mathematical form of Hill's yield criterion would be used in this investigation. Despite von Mises yield criterion, which may be

employed in any arbitrary coordinate system, Hill's yield criterion is only applicable in the system in which material has threefold symmetry about that. However, only the mathematical form of Hill's yield criterion is used here, and the coordinate system is taken to be the same for all grains coincident with the global xyz frame; therefore, this is no limitation in this study (see the notes in the last lines of Appendix A.3).

$$F(\sigma_{yy} - \sigma_{zz})^2 + G(\sigma_{zz} - \sigma_{xx})^2 + H(\sigma_{xx} - \sigma_{yy})^2 + 2L\tau_{yz}^2 + 2M\tau_{xz}^2 + 2N\tau_{xy}^2 = 1 \quad (2)$$

F, G, H, \dots, N in Eq. (2) are constants that depend on the material's normal and shear strength. Eq. (3) to Eq. (8) are relations [32] describing constants of Eq. (2) in terms of σ_{ii}^y (no sum on i) for normal stresses and k_{ij}^y for shear stress. σ_{ii}^y or k_{ij}^y represent the material's yield strength when the only non-zero component of stress is σ_{ii} or τ_{ij} .

$$F = \frac{1}{2} \left[\frac{1}{(\sigma_{yy}^y)^2} + \frac{1}{(\sigma_{zz}^y)^2} - \frac{1}{(\sigma_{xx}^y)^2} \right] \quad (3)$$

$$G = \frac{1}{2} \left[\frac{1}{(\sigma_{xx}^y)^2} + \frac{1}{(\sigma_{zz}^y)^2} - \frac{1}{(\sigma_{yy}^y)^2} \right] \quad (4)$$

$$H = \frac{1}{2} \left[\frac{1}{(\sigma_{xx}^y)^2} + \frac{1}{(\sigma_{yy}^y)^2} - \frac{1}{(\sigma_{zz}^y)^2} \right] \quad (5)$$

$$L = \frac{1}{2(k_{yz}^y)^2} \quad (6)$$

$$M = \frac{1}{2(k_{xz}^y)^2} \quad (7)$$

$$N = \frac{1}{2(k_{xy}^y)^2} \quad (8)$$

Thus far, it is shown that it would be possible to calculate the strength of grain with the defined orientation using the Taylor factor. In order to evaluate σ_{ii}^y and k_{ij}^y for each grain, six different Taylor factors corresponding to six different global strain tensors (i.e. $[E]$) must be calculated. For example, in order to calculate

the yield strength of grain in the x -direction (σ_{xx}^y), $[E]$ must be placed as $[E] = \text{diag}[1, -0.5, -0.5]$, the resulting value of the Taylor factor would be M_{xx} so the strength of that grain in x -direction would be $\sigma_{xx}^y = M_{xx}\tau_{CRSS}$. In order to calculate the shear yield strength of that grain in xy -plane (k_{xy}^y), $[E]$ must be placed as

$$[E] = \begin{bmatrix} 0 & 1 & 0 \\ 1 & 0 & 0 \\ 0 & 0 & 0 \end{bmatrix}$$

, the resulting value of the Taylor factor would be M_{xy} , and based on Eq. (1), the effective stress due to shear stress at the onset of yielding would be $\sigma_{xy}^y = M_{xy}\tau_{CRSS}$. Therefore, the shear strength of that grain in xy -plane would be

$$k_{xy} = 1/\sqrt{3} \sigma_{xy}^y = 1/\sqrt{3} M_{xy}\tau_{CRSS}$$

Proceeding the same routine and calculating other terms (M_{yy} , M_{zz} , M_{xz} and M_{yz}), one may use Hill's yield criterion for grain in aggregate with the following coefficients:

$$F = \frac{1}{2\tau_{CRSS}^2} \left(\frac{1}{M_{yy}^2} + \frac{1}{M_{zz}^2} - \frac{1}{M_{xx}^2} \right) \quad (9)$$

$$G = \frac{1}{2\tau_{CRSS}^2} \left(\frac{1}{M_{zz}^2} + \frac{1}{M_{xx}^2} - \frac{1}{M_{yy}^2} \right) \quad (10)$$

$$H = \frac{1}{2\tau_{CRSS}^2} \left(\frac{1}{M_{xx}^2} + \frac{1}{M_{yy}^2} - \frac{1}{M_{zz}^2} \right) \quad (11)$$

$$L = \frac{1}{\tau_{CRSS}^2} \frac{3}{2M_{yz}^2} \quad (12)$$

$$M = \frac{1}{\tau_{CRSS}^2} \frac{3}{2M_{xz}^2} \quad (13)$$

$$N = \frac{1}{\tau_{CRSS}^2} \frac{3}{2M_{xy}^2} \quad (14)$$

2.2. Experimental Study

The experimental procedure of this study consists of 1) the production of fine and coarse-grained copper miniature rods and 2) the microforging of these miniature rods.

2.2.1. Development and characterization of fine and coarse-grained rods

Two copper rods with 10mm in diameter underwent the circular simple shear extrusion (CSSE) [33-35] process for eight passes to produce ultrafine-grained rods. Based on our previously published investigations [36], the grain size was expected to scale down to 1 μ m. To produce coarse-grained rods, one of the SPDed copper rods, annealed at 950 °C for 24hrs, resulted in a grain size of about 70 μ m. To obtain the mechanical properties of these rods, a cylinder with the dimensions of 6mm in diameter and 9mm in length was machined out of each rod, and the compression test with Teflon as a lubricant was performed. To establish $\tau_{CRSS} - \gamma$ curve, the following fact was considered: the average Taylor factor for a material with fcc crystal structure made of numerous randomly oriented grains is about 3.067, so based on Eq. (1), if the values of the stress are divided by 3.067 and the values of the strain are multiplied by 3.067, the dependence of τ_{CRSS} on γ would be obtained, where γ is the total shear strain on active slip systems [37].

2.2.2. Microforging of the miniature rods

Miniature rods 1mm in diameter and nearly 5mm in length were cut out of both annealed and SPDed rods by wire-cut. These rods are then microforged into equilateral triangular prismatic pieces by means of the die set shown in Fig. 1. The insert is plugged at the bottom of the die hole, then a miniature rod is placed above the insert and compressed by the punch to fill the die cavity. After that, the insert is unplugged, and the formed specimen is taken out.

2.3. Finite Element Simulation

2.3.1. Simulation of microforging of SPDed miniature rods

Based on the work of Bagherpour et al. [30], processing of material with SSE results in developing a multi-component simple shear texture that partially recovers due to the phenomenon of strain reversal [38]. However, the presence of such a weak, multi-components texture would not be expected to affect the successful microforging of specimens, and due to the presence of numerous ultrafine grains in each cross-section

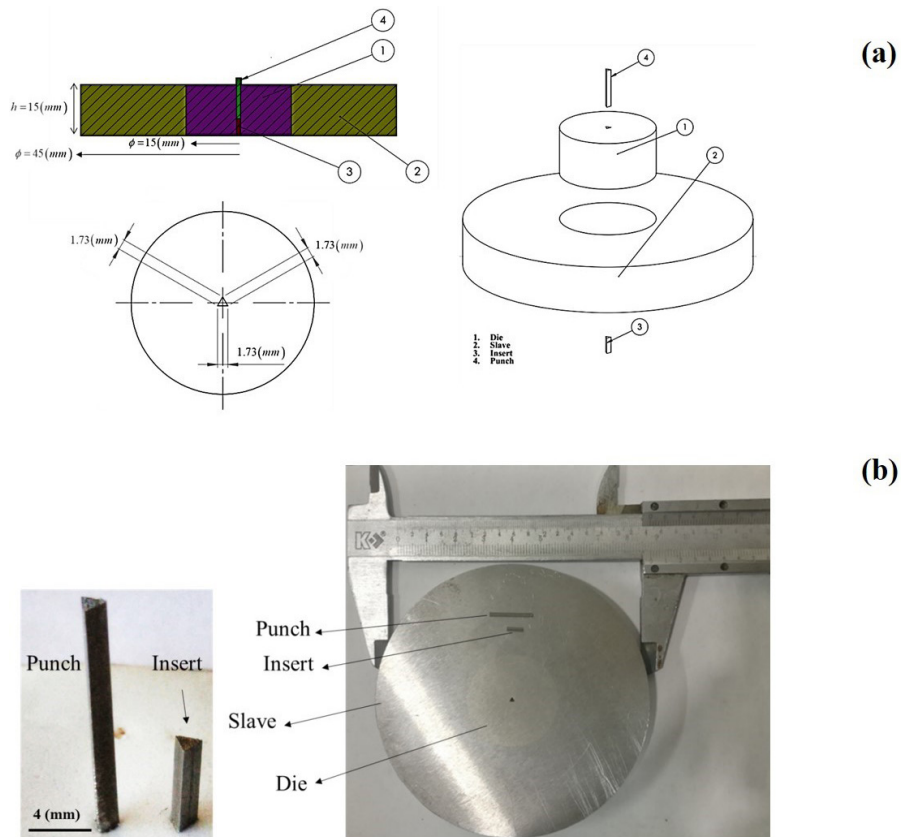


Fig. 1- Microforging die set a) CAD sketch and b) real parts.

of the material, the behavior of material would be expected to be repeatable without any traces of the size effect. Besides, it is well-known that the texture has primary importance in the sheet metal forming processes and less affects the bulk metal forming processes (such as microforging in this study). Based on these logics, it is assumed that the weak, multi-component texture does not affect the forming loads under the multiaxial state of stress that prevails in the closed-die forging. Hence, for the sake of simplicity, the microforging process is simulated by conventional routine, which means assigning von Mises flow potential to the material and assuming the material to be isotropic without partitioning the specimen.

2.3.2. Upper and lower bounds of load-normalized displacement curves of microforging of annealed specimens

Precise examination of the proposed model requires sophisticated experimental and computational tools. It is required that the microstructure of a specimen is fully reconstructed in the FE software, and the load-displacement and strain distribution predicted by FE analysis be compared with the experimental results. However, in order to evaluate the proposed model to some

degree, initially, the stiffest and the most compliant orientations for this particular forming process are determined (Table 1 and Fig. 2.b) (the procedure is discussed in the appendix, section A.2). Then the values of M_{ij} s corresponding to the stiffest orientation are used to calculate F, G, \dots, N . The simulation in this condition gives the upper limit of the force-displacement curve; similarly, the lower bound of force-displacement could be obtained. Since the phenomenon of size effect becomes bold as the grain size increases, different force-displacement curves are expected from different annealed specimens. If the experimental results were enveloped by these bounds, the model's validity could be roughly ensured.

The assigned $\tau_{CRSS} - \gamma$ curve corresponds to the annealed material obtained from the compression test, as discussed in section 2.2.1. It is necessary to state that in this model, the effect of grain size on the flow stress of the material is considered through the proper definition of $\tau_{CRSS} - \gamma$. Keeping the same $\tau_{CRSS} - \gamma$ as the input to the FE code, creating grain boundaries by partitioning the specimen only divides the material into segments which without assigning different orientations to these segments, flow stress of the material would not be affected. Therefore, as in these simulations, the goal is to

Table 1- Introduction of the stiffest and the most compliant orientations

	Euler angles ($\varphi_1, \Phi, \varphi_2$)	M_{xx}	M_{yy}	M_{zz}	M_{xy}
Stiffest Orientation	(345, 125, 137)	3.2389	3.4022	3.6688	3.3271
The most compliant Orientation	(113, 88, 261)	2.5730	2.6554	2.3521	3.4180

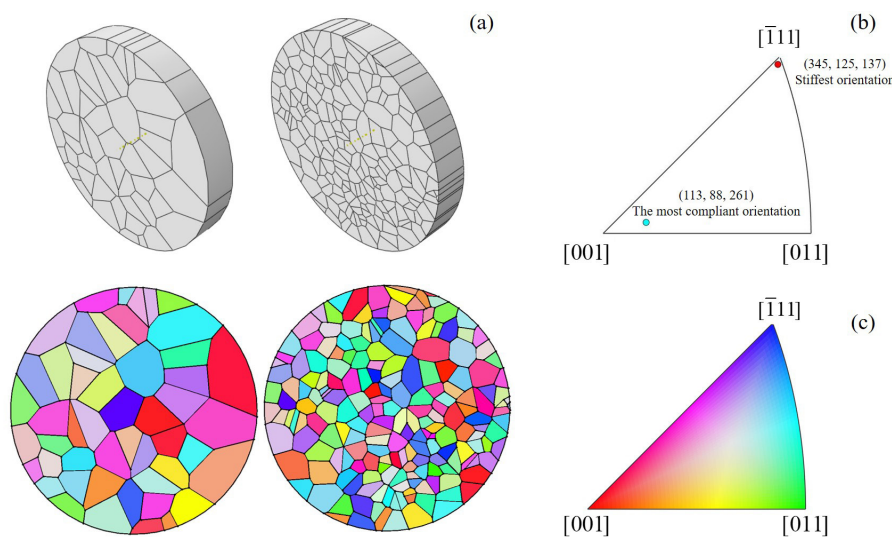


Fig. 2- (a) specimens composed of 50 and 200 grains in their cross-section, (b) representation of stiffest and the most compliant orientations in the unit triangle, and (c) color coded orientation map of specimens.

simulate a situation where all grains are oriented in the stiffest or the most compliant orientations; the designed specimen is not partitioned into cells. Instead, the R_{ij} correspond to the stiffest or the most compliant orientation are assigned to the whole cylindrical specimen with the same geometry as the experimental micro-rods.

2.3.3. Simulation of the microforging of specimens composed of 50 and 200 grains in the cross-section

As stated above, the proposed model makes it possible to investigate the effect of grain size on the statistical representation of the specimen without interfering effects of grain size on the flow stress and work hardening exponent. This is beneficial since the variation in the work hardening exponent may alter the strain distribution as well.

Here, this ability is used to study the co-effect of grain size and the requirement of preserving continuity on the distribution of plastic strain in the specimen. In order to execute these simulations, first, the cross-section of the designed rods is partitioned into 50 and 200 Voronoi cells, as shown in Fig. 2.a. Then, a random orientation is assigned to each grain where the corresponding color coded orientation maps are shown in Fig. 2.c. The six Taylor factors for each grain are calculated using the numerical procedure explained in appendix A.1, and the constants of Hill's yield criterion are then calculated using Eq. (9-14). The material axis required to implement Hill's yield criterion was chosen to be the same for all grains, coincident with the global xyz frame. In order to eliminate the effect of the work-hardening exponent on the distribution of strain, a constant value of τ_{CRSS} without dependency on γ (perfect plastic) is assigned to the material for simulation.

2.4. Validation of convexity

It has been shown by Bishop and Hill [39] that

each proposed yield criterion for a material that deforms plastically by the slip must be convex. Investigating the convexity of a multivariable function is usually done by the Hessian matrix.

3. Results and Discussion

3.1. Concavity of the Combined Hill-Taylor model

The Hessian matrix of the combined Hill-Taylor model is as shown in Eq. (15), factoring the term $1/(\tau_{CRSS}^2)$ that is independent of M_{ij} s. (15)

$$\begin{bmatrix} \frac{2}{M_{xx}^2} \left(\frac{1}{M_{zz}^2} - \frac{1}{M_{yy}^2} - \frac{1}{M_{xx}^2} \right) \left(\frac{1}{M_{yy}^2} - \frac{1}{M_{xx}^2} - \frac{1}{M_{zz}^2} \right) & 0 & 0 & 0 \\ \text{sym.} & \frac{2}{M_{yy}^2} \left(\frac{1}{M_{xx}^2} - \frac{1}{M_{yy}^2} - \frac{1}{M_{zz}^2} \right) & 0 & 0 & 0 \\ \text{sym.} & \text{sym.} & \frac{2}{M_{zz}^2} & 0 & 0 & 0 \\ \text{sym.} & \text{sym.} & \text{sym.} & \frac{6}{M_{xy}^2} & 0 & 0 \\ \text{sym.} & \text{sym.} & \text{sym.} & \text{sym.} & \frac{6}{M_{yz}^2} & 0 \\ \text{sym.} & \text{sym.} & \text{sym.} & \text{sym.} & \text{sym.} & \frac{6}{M_{zx}^2} \end{bmatrix}$$

The corresponding eigenvalues of this matrix are shown in Eq. (16), where λ_i s correspond to eigenvalues. It can be seen that all components are non-negative in all ranges of M_{ij} s except for λ_5 . In Fig. 3, color filled contours of the variations of λ_5 with M_{xx} and M_{yy} are plotted for three values of M_{zz} , which are $M_{zz}|_{min}=2.3$, $M_{zz}|_{max}=3.674$ and $M_{zz}|_{mean}=[M_{zz}|_{max} + M_{zz}|_{min}]/2=2.987$. As it can be seen, neither of those values would result in λ_5 to have a negative value in the range of $\{2.3 \leq M_{xx}, M_{yy} \leq 3.674\}$. Therefore, it can be concluded that in the physically meaningful range of the variations of M_{xx} , M_{yy} and M_{zz} all eigenvalues of the Hessian matrix of the proposed model are non-negative. Hence, the Hessian matrix is positive semi-definite and based on the work of Tong [40],

$$\begin{bmatrix} \lambda_1 \\ \lambda_2 \\ \lambda_3 \\ \lambda_4 \\ \lambda_5 \\ \lambda_6 \end{bmatrix} = \begin{bmatrix} 0 \\ 6/M_{xy}^2 \\ 6/M_{xz}^2 \\ 6/M_{yz}^2 \\ \frac{M_{xx}^2 M_{yy}^2 + M_{xx}^2 M_{zz}^2 + M_{yy}^2 M_{zz}^2 - 2\sqrt{M_{xx}^4 M_{yy}^4 + M_{xx}^4 M_{zz}^4 + M_{yy}^4 M_{zz}^4} - M_{xx}^2 M_{yy}^2 M_{zz}^4 - M_{xx}^2 M_{zz}^2 M_{yy}^4 - M_{yy}^2 M_{zz}^2 M_{xx}^4}{M_{xx}^2 M_{yy}^2 M_{zz}^2} \\ \frac{M_{xx}^2 M_{yy}^2 + M_{xx}^2 M_{zz}^2 + M_{yy}^2 M_{zz}^2 + 2\sqrt{M_{xx}^4 M_{yy}^4 + M_{xx}^4 M_{zz}^4 + M_{yy}^4 M_{zz}^4} - M_{xx}^2 M_{yy}^2 M_{zz}^4 - M_{xx}^2 M_{zz}^2 M_{yy}^4 - M_{yy}^2 M_{zz}^2 M_{xx}^4}{M_{xx}^2 M_{yy}^2 M_{zz}^2} \end{bmatrix} \quad (16)$$

the proposed model is convex.

In another study, Pankaj et al. [44] established a condition for convexity of Hill's yield criterion with a different methodology. Their inequality that is shown by Eq. (17) is obtained based on Hill's yield criterion to be an ellipse in the deviatoric plane.

$$FG + GH + HF > 0 \tag{17}$$

Using Eq. (9) to Eq. (11), factoring the term $1/(\tau_{CRSS}^2)$ that is independent of M_{ij} and making some simplifications, Eq. (17) reduces to: (18)

$$2M_{xx}^4 M_{yy}^2 M_{zz}^2 + 2M_{xx}^2 M_{yy}^4 M_{zz}^2 + 2M_{xx}^2 M_{yy}^2 M_{zz}^4 > M_{xx}^4 M_{yy}^4 + M_{xx}^4 M_{zz}^4 + M_{yy}^4 M_{zz}^4$$

On the other hand, as it can be seen in Eq. (16), the necessary condition for λ_5 to be positive is as Eq. (19).

Raise the power of both sides by 2 and performing some simplifications, it can be seen that both of these conditions are the same. This conformity proves that the mathematical procedure adopted in this work to study the convexity of the proposed

$$M_{xx}^2 M_{zz}^2 + M_{yy}^2 M_{zz}^2 + M_{xx}^2 M_{yy}^2 > 2\sqrt{M_{xx}^4 M_{yy}^4 - M_{xx}^4 M_{yy}^2 M_{zz}^2 + M_{xx}^4 M_{zz}^4 - M_{xx}^2 M_{yy}^4 M_{zz}^2 - M_{xx}^2 M_{yy}^2 M_{zz}^4 + M_{yy}^4 M_{zz}^4} \tag{19}$$

model is valid.

The problem of identifying the model constants preserving the convexity is challenging, and much effort has been focused on that, for example, works of Tong [41] and Uppaluri and Helm [42]. However, while Hill's yield criterion constants are calculated for individual grains in this scheme, the idea can be employed to determine the constants of other models such as Gotoh [43]. This could be established by calculating average Taylor factors, provided that the material's texture is identified or a random texture is assigned to the material.

3.2. Compression test

In Fig. 4, the true stress-strain curves of both SPDed and annealed specimens are shown. It can be seen that after eight passes of CSSE, the processed material is saturated with cold working in a way that the flow stress is about 350 MPa without any further hardening. This is in complete accordance with studies on other SPD techniques (e.g., Pardis et al. [45]). Annealing the deformed specimens resulted in the flow stress to decrease and the recovery of the work hardening. For each case, the

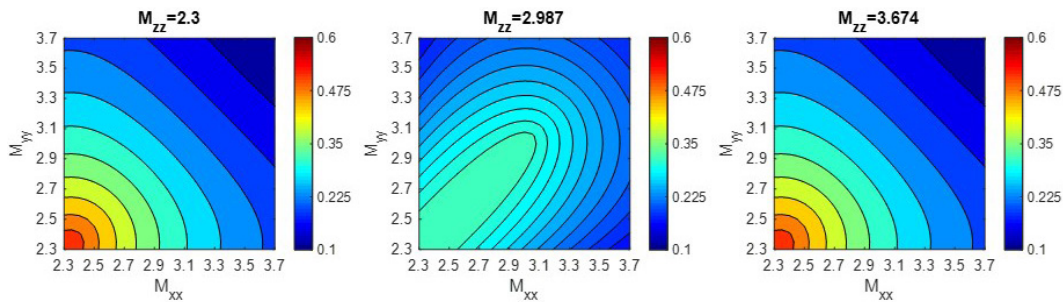


Fig. 3- Color filled contours of variation of λ_5 with M_{xx} and M_{yy} for three values of M_{zz} .

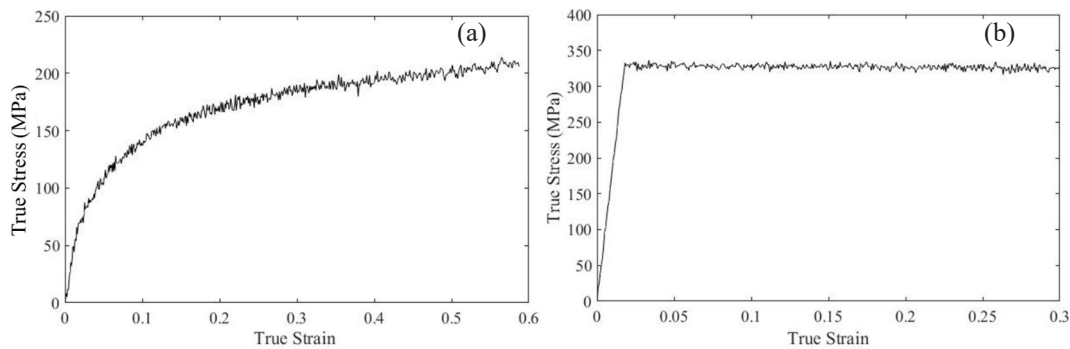


Fig. 4- True stress-strain for a) annealed copper and b) SPDed copper.

values of stress are divided by 3.067, and the values of strain are multiplied by 3.067 to obtain $\tau_{CRSS} - \gamma$, which is used further as the mechanical behavior of the material in simulation.

3.3. Microforging of SPDeD miniature rods: experimental and FE results

In Fig. 5, the load-normalized displacement curves for the microforging of SPDeD miniature rods are shown. To calculate normalized displacement, the current values of displacement are divided by the final value of displacement for which the forging process is completed. It can be seen that the results of the simulation are in good agreement with the experimental results.

3.4. Microforging of annealed miniature rods: experimental and FE results

Fig. 6 shows the load-normalized displacement of the microforging of annealed miniature rods. It can be seen that the load-displacement curves corresponding to the stiffest and most compliant situations well envelope the experimental data in a wide range of processes. However, the curves collided at the end of the process. The main reason is that as large strains are imposed on the material, the proposed combined Hill-Taylor model would not be valid. Since in this model, the lattice rotation phenomenon did not take into account, and the orientation of an individual grain is far different from its original orientation. Therefore, the calculated M_{ij} s, which were based on the initial orientation of the grain, are no longer applicable.

The difference between the load-displacement curves of the two experimentally microforged specimens in Fig. 6 is due to the size effect. The average grain size of the annealed grains was

measured to be about 70µm. This means that in each cross-section of the annealed miniature rods, approximately 200 grains were present. Based on the work of Henning & Vehoff [15], if the number of grains in each cross-section is fewer than 100~200, the size effect reveals. The following case was laid on the edge of this threshold, and therefore, the difference between the load-displacement curves of the two specimens was not as much as expected.

3.5. Microforging of specimens with a different number of grains in their cross-section: FE results

Fig. 7 shows the results of the simulation of specimens with 50 and 200 grains in their cross-section. The final cross-section of the specimens and distribution of equivalent plastic strain in the cross-section of these two specimens are shown. It can be seen that the proposed model successfully captures the fact that due to the difference in the mechanical behavior of the grains, the distribution of the equivalent plastic strain abruptly varies from one grain to another. Similar behavior is observed by the digital image correlation (DIC) technique for plane strain compression of pure Al in the work of Raabe et al. [46] and through the simulations with different methodology in the works of Knezevic et al. and Vidyasagar et al. [47,48].

Based on the literature, one aspect of the size effect is the statistical representation of the specimen, which is emphasized in the works of Henning & Vehoff and Chan et al. [15,17]. In the circumstances where the number of grains in the cross-section is relatively low, the individual behavior of each grain determines the flow behavior of the material at regions with length scales comparable to the specimen size. Therefore, an overall inhomogeneity

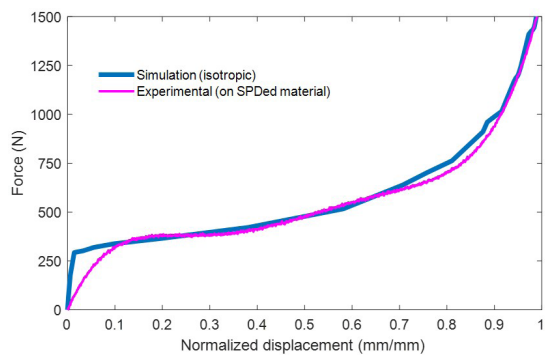


Fig. 5- Load-normalized displacement curves for the microforging of the SPDeD specimens obtained by simulation and experiment.

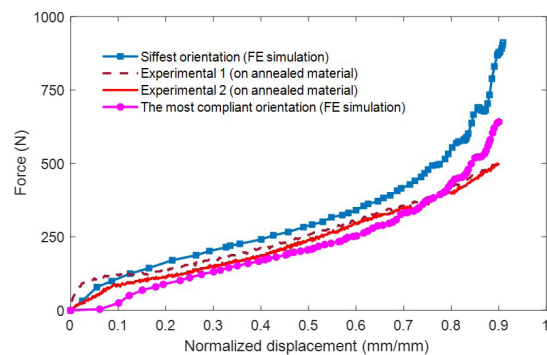


Fig. 6- Load-normalized displacement curves of the microforging of the annealed specimens obtained by simulation and experiments.

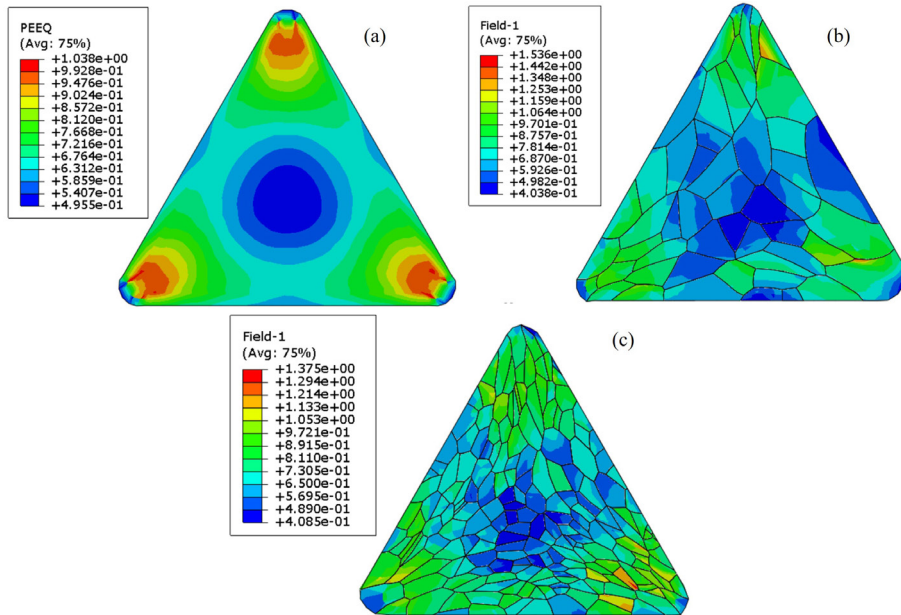


Fig. 7- Distribution of equivalent plastic strain on final cross-section (a) isotropic specimen, (b) specimen with 50 grains in the cross-section, and (c) specimen with 200 grains in the cross-section.

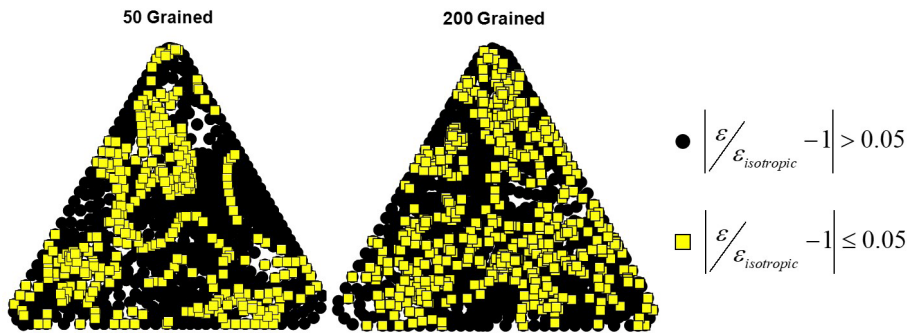


Fig. 8- Illustration of the points in material with $\epsilon/\epsilon_{isotropic}$ between 0.95 and 1.05 (yellow squares) and points for which $\epsilon/\epsilon_{isotropic}$ is over 1.05 or below 0.95 (black circles) for a) specimen with 50 grains in its cross-section and b) specimen with 200 grains in its cross-section.

is predominant in the specimen at large length scales. As the number of grains in the cross-section of the specimen increases, this length scale is shortened to the point that the individual behaviors of grains do not determine the flow of material at length scales comparable to the specimen size. In this circumstance, an overall homogeneity would be established.

On the other hand, from the geometrical point of view, the grains that are oriented in a manner compliant with the deformation of material are required to compensate for the deformation of the grains oriented in an in compliant manner, hence experiencing larger strains to maintain continuity. It can be concluded from the work of Ashby [8] that preserving such compatibility is harder to

accomplish between larger grains. Hence, it is expected that by increasing the number of grains in the cross-section, the equivalent plastic strain in each location shifts toward the one for the isotropic case both in the viewpoint of statistics and geometry.

Based on the above discussion, the ratio of the equivalent plastic strain in the specimens composed of a different number of grains in their cross-section (ϵ) to the equivalent plastic strain for the case of the isotropic specimen ($\epsilon_{isotropic}$) is calculated point-by-point for each specimen. In Fig. 8, based on the magnitude of $\epsilon/\epsilon_{isotropic}$, two type of points can be distinguished:

a) Yellow squares: where the difference between the equivalent plastic strain at a particular point bounds between 0.95 to 1.05 of equivalent plastic strain

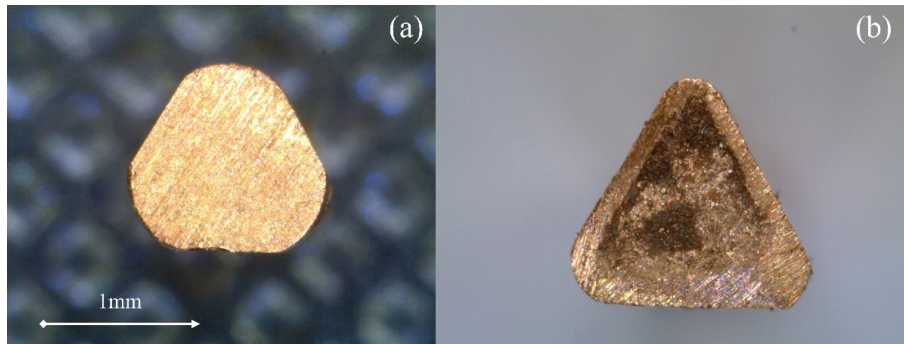


Fig. 9- Successfully produced microparts from SPDed miniature rods (a) in the middle stages of deformation and (b) in the final stage.

at the same point if the material were isotropic (consisted of a virtually infinite number of grains).
 b) Black circles: where this ratio is below 0.95 or above 1.05.

It can be seen that increasing the number of grains in the cross-section led to more points having the ratio in the range of 0.95 to 1.05 (near unity), which means more points experience plastic equivalent strains similar to the case of the isotropic specimen. This is in accordance with the expectations and emphasizes that the proposed model well conforms with the statistical and geometrical features of the phenomenon of size effect.

From a practical point of view, inhomogeneity in the large-grained specimens may cause deficiencies such as cracks and flaws. Hence, it can be concluded that the successful production of microparts requires that the raw material be a product of processes resulting in grain refinement, such as SPD techniques [49,50]. Fig. 9 shows the successful microforging of SPDed miniature rod to the desired final shape.

4. Conclusion

In this paper, by combining the crystal plasticity notions developed by Taylor and the mathematical form of Hill's yield criterion, a model was developed that can be used to describe the plasticity of grains. The main benefit of this model is that it can be operated in many commercial FE codes without further coding. The main findings include:

- It is shown that the proposed Hill-Taylor model fulfills the condition of convexity.
- The upper and lower bounds for the load-displacement of the microforging of annealed miniature copper rods are established by the FE simulation. It was observed that the experimental data lay between these bounds to a vast extent; therefore, the validity of the model can roughly be

ensured.

- The simulation of microforging of specimens with a different number of grains in the cross-section (50 and 200) showed that the proposed model validly captures the fact that by increasing the number of grains in the cross-section, plastic equivalent strain tends toward that for the case of isotropic material.
- Based on the results, it can be concluded that the successful production of microparts by forming processes requires that the microstructure of the raw material be refined by proper methods such as the SPD techniques.

Acknowledgments

The authors appreciate Shiraz University for its financial support (Grant numbers of 98-GR-ENG-15) and research facilities used in this work.

References

1. Schmid E, Boas W. *Plasticity of crystals : with special reference to metals*: Chapman & Hall; 1968.
2. Sachs G. Plasticity problems in metals. *Transactions of the Faraday Society*. 1928;24:84.
3. Cox HL, Sopwith DG. The effect of orientation on stresses in single crystals and of random orientation on strength of polycrystalline aggregates. *Proceedings of the Physical Society*. 1937;49(2):134-51.
4. Taylor GI. Plastic Strain in Metals. *The Journal of the Institute of Metals*. 1938; 62, 307-324
5. Taylor GI. Analysis of plastic strain in a cubic crystal. *Stephen Timoshenko 60th Anniversary Volume*. 1938:218-24.
6. Taylor GI, Elam CF. Bakerian Lecture: The distortion of an aluminium crystal during a tensile test. *Proceedings of the Royal Society of London Series A, Containing Papers of a Mathematical and Physical Character*. 1923;102(719):643-67.
7. Bishop JFW, Hill R. XLVI. A theory of the plastic distortion of a polycrystalline aggregate under combined stresses. *The London, Edinburgh, and Dublin Philosophical Magazine and Journal of Science*. 1951;42(327):414-27.
8. Ashby MF. The deformation of plastically non-homogeneous materials. *The Philosophical Magazine: A Journal of Theoretical Experimental and Applied Physics*. 1970;21(170):399-424.
9. Fleck NA, Muller GM, Ashby ME, Hutchinson JW. Strain gradient plasticity: Theory and experiment. *Acta Metallurgica et*

- Materialia. 1994;42(2):475-87.
10. Nye JF. Some geometrical relations in dislocated crystals. *Acta Metallurgica*. 1953;1(2):153-62.
 11. Ran JQ, Fu MW, Chan WL. The influence of size effect on the ductile fracture in micro-scaled plastic deformation. *International Journal of Plasticity*. 2013;41:65-81.
 12. Li WT, Fu MW, Shi SQ. Study of deformation and ductile fracture behaviors in micro-scale deformation using a combined surface layer and grain boundary strengthening model. *International Journal of Mechanical Sciences*. 2017;131-132:924-37.
 13. Li J, Romero I, Segurado J. Development of a thermo-mechanically coupled crystal plasticity modeling framework: Application to polycrystalline homogenization. *International Journal of Plasticity*. 2019;119:313-30.
 14. Li WT, Li H, Fu MW. Interactive effect of stress state and grain size on fracture behaviours of copper in micro-scaled plastic deformation. *International Journal of Plasticity*. 2018;114:126-43.
 15. Henning M, Vehoff H. Statistical size effects based on grain size and texture in thin sheets. *Materials Science and Engineering: A*. 2007;452-453:602-13.
 16. Chen G, Zhang L, Bezold A, Broeckmann C, Weichert D. Statistical investigation on influence of grain size on effective strengths of particulate reinforced metal matrix composites. *Computer Methods in Applied Mechanics and Engineering*. 2019;352:691-707.
 17. Chan WL, Fu MW, Lu J, Liu JG. Modeling of grain size effect on micro deformation behavior in micro-forming of pure copper. *Materials Science and Engineering: A*. 2010;527(24-25):6638-48.
 18. Cortellino F, Rouse JP, Cacciapuoti B, Sun W, Hyde TH. Experimental and Numerical Analysis of Initial Plasticity in P91 Steel Small Punch Creep Samples. *Exp Mech*. 2017;57(8):1193-212.
 19. Hollang L, Hieckmann E, Brunner D, Holste C, Skrotzki W. Scaling effects in the plasticity of nickel. *Materials Science and Engineering: A*. 2006;424(1-2):138-53.
 20. Hua F, Liu D, Li Y, He Y, Dunstan DJ. On energetic and dissipative gradient effects within higher-order strain gradient plasticity: Size effect, passivation effect, and Bauschinger effect. *International Journal of Plasticity*. 2021;141:102994.
 21. Jiang J, Britton TB, Wilkinson AJ. The orientation and strain dependence of dislocation structure evolution in monotonically deformed polycrystalline copper. *International Journal of Plasticity*. 2015;69:102-17.
 22. Kraft O, Gruber PA, Mönig R, Weygand D. Plasticity in Confined Dimensions. *Annual Review of Materials Research*. 2010;40(1):293-317.
 23. Lu X, Zhang X, Shi M, Roters F, Kang G, Raabe D. Dislocation mechanism based size-dependent crystal plasticity modeling and simulation of gradient nano-grained copper. *International Journal of Plasticity*. 2019;113:52-73.
 24. Ravaji B, Joshi SP. A crystal plasticity investigation of grain size-texture interaction in magnesium alloys. *Acta Materialia*. 2021;208:116743.
 25. Zhang B, Dodaran MS, Shao S, Choi J, Park S, Meng WJ. Understanding of plasticity size-effect governed mechanical response and incomplete die filling in a microscale double-punch molding configuration. *International journal of mechanical sciences*. 2020;172:105406.
 26. Yang LH, Zou GP, Qu J. Yield Criterion and Crack Tip Plastic Zone of Nickel-Based Single Crystal. *Key Engineering Materials*. 2012;525-526:341-4.
 27. Zhang K, Holmedal B, Mánik T, Saai A. Assessment of advanced Taylor models, the Taylor factor and yield-surface exponent for FCC metals. *International Journal of Plasticity*. 2019;114:144-60.
 28. Kim HL, Park SH. Loading Direction Dependence of Yield-Point Phenomenon and Bauschinger Effect in API X70 Steel Sheet. *Metals and Materials International*. 2019;26(1):14-24.
 29. Zhang S, Liu Y, Xu T, Sun M, Zhang Q, Wan Y. Effect of Texture and Microstructure on Tensile Behaviors in the Polycrystalline Pure Niobium. *Metals and Materials International*. 2021;27(10):4023-34.
 30. Bagherpour E, Qods F, Ebrahimi R, Miyamoto H. Microstructure and Texture Inhomogeneity after Large Non-Monotonic Simple Shear Strains: Achievements of Tensile Properties. *Metals*. 2018;8(8):583.
 31. A theory of the yielding and plastic flow of anisotropic metals. *Proceedings of the Royal Society of London Series A Mathematical and Physical Sciences*. 1948;193(1033):281-97.
 32. Johnson W, Mellor PB. *Engineering plasticity* (pp. 76–78). 1983. England: Ellis Horwood Ltd.
 33. Ebrahimi R, Rezvani A, Bagherpour E. Circular simple shear extrusion as an alternative for simple shear extrusion technique for producing bulk nanostructured materials. *Procedia Manufacturing*. 2018;15:1502-8.
 34. Rezvani A, Ebrahimi R. Investigation on the Deformation Behavior and Strain Distribution of Commercially Pure Aluminum after Circular Simple Shear Extrusion. *Journal of Ultrafine Grained and Nanostructured Materials*. 2019 Jun 1;52(1):32-42.
 35. Rezvani A, Bagherpour E, Ebrahimi R. Circular Simple Shear Extrusion as an Alternative to Simple Shear Extrusion Technique. *Iranian Journal of Science and Technology, Transactions of Mechanical Engineering*. 2018;44(1):193-201.
 36. Bagherpour E, Qods F, Ebrahimi R, Miyamoto H. Microstructure quantification of ultrafine grained pure copper fabricated by simple shear extrusion (SSE) technique. *Materials Science and Engineering: A*. 2016;674:221-31.
 37. Hosford WF. *Mechanical Behavior of Materials*: Cambridge University Press; 2009.
 38. Bagherpour E, Qods F, Ebrahimi R, Miyamoto H. Microstructure evolution of pure copper during a single pass of simple shear extrusion (SSE): role of shear reversal. *Materials Science and Engineering: A*. 2016;666:324-38.
 39. Bishop JFW, Hill R. CXXVIII. A theoretical derivation of the plastic properties of a polycrystalline face-centred metal. *The London, Edinburgh, and Dublin Philosophical Magazine and Journal of Science*. 1951;42(334):1298-307.
 40. Tong W. Algebraic Convexity Conditions for Gotoh's Nonquadratic Yield Function. *Journal of Applied Mechanics*. 2018;85(7).
 41. Tong W. On the Certification of Positive and Convex Gotoh's Fourth-Order Yield Function. *Journal of Physics: Conference Series*. 2018;1063:012093.
 42. Uppaluri R, Helm D. A convex fourth order yield function for orthotropic metal plasticity. *European Journal of Mechanics - A/Solids*. 2021;87:104196.
 43. Gotoh M. A theory of plastic anisotropy based on a yield function of fourth order (plane stress state)—I. *International Journal of Mechanical Sciences*. 1977;19(9):505-12.
 44. Pankaj, Arif M, Kaushik SK. Convexity studies of two anisotropic yield criteria in principal stress space. *Engineering Computations*. 1999;16(2):215-29.
 45. Pardis N, Chen C, Ebrahimi R, Toth LS, Gu CF, Beausir B, et al. Microstructure, texture and mechanical properties of cyclic expansion–extrusion deformed pure copper. *Materials Science and Engineering: A*. 2015;628:423-32.
 46. Raabe D, Sachtleber M, Zhao Z, Roters F, Zaeferrer S.

Micromechanical and macromechanical effects in grain scale polycrystal plasticity experimentation and simulation. Acta Materialia. 2001;49(17):3433-41.

47. Knezevic M, Drach B, Ardeljan M, Beyerlein IJ. Three dimensional predictions of grain scale plasticity and grain boundaries using crystal plasticity finite element models. Computer Methods in Applied Mechanics and Engineering. 2014;277:239-59.

48. Vidyasagar A, Tutcuoglu AD, Kochmann DM. Deformation patterning in finite-strain crystal plasticity by spectral homogenization with application to magnesium. Computer Methods in Applied Mechanics and Engineering. 2018;335:584-609.

49. Khajezade A, HABIBI PM, Mirzadeh H, MONTAZERI PM. Grain refinement efficiency of multi-axial incremental forging and shearing: A Crystal Plasticity Analysis.

50. Torabi M, Eivani AR, Jafarian H, Salehi MT. Re-strengthening in AA6063 alloy during equal channel angular pressing. Journal of Ultrafine Grained and Nanostructured Materials. 2017 Dec 1;50(2):90-7.

51. Van Houtte P, Wagner F. Development of Textures by Slip and Twinning. Preferred Orientation in Deformed Metal and Rocks: Elsevier; 1985. p. 233-58.

52. W. F. Hosford. The mechanics of crystals and textured polycrystals. Oxford University Press, New York–Oxford 1993. ISBN 9780195077445.

53. Zadeh L. Optimality and non-scalar-valued performance criteria. IEEE Transactions on Automatic Control. 1963;8(1):59-60.

54. Goicoechea A, Duckstein L, Fogel MM. Multiobjective programming in watershed management: A study of the Charleston Watershed. Water Resources Research. 1976;12(6):1085-92.

Appendix

A. 1. Calculation of Taylor factor

Suppose a crystal in a crystal aggregate oriented by Euler angles of $(\varphi_1, \Phi, \varphi_2)$ to any fixed global coordinate system, xyz . If the crystal aggregate is stressed, according to Taylor's hypothesis, one must do the following procedure to calculate the strength of that individual grain:

1- Formation of the global strain as:

$$[E] = \begin{bmatrix} de_{xx} & de_{xy} & de_{xz} \\ sym. & de_{yy} & de_{yz} \\ sym. & sym. & de_{zz} \end{bmatrix} \quad (A. 1)$$

Where $[E]$ represents global strain tensor.

2- Transformation of the global strain tensor into crystal coordinate system by using rotation tensor with the form of [51]:

$$[R] = \begin{bmatrix} \cos \varphi_1 \cos \varphi_2 - \sin \varphi_1 \sin \varphi_2 \cos \Phi & \sin \varphi_1 \cos \varphi_2 + \cos \varphi_1 \sin \varphi_2 \cos \Phi & \sin \varphi_2 \sin \Phi \\ -\cos \varphi_1 \sin \varphi_2 - \sin \varphi_1 \cos \varphi_2 \cos \Phi & -\sin \varphi_1 \sin \varphi_2 + \cos \varphi_1 \cos \varphi_2 \cos \Phi & \cos \varphi_2 \sin \Phi \\ \sin \varphi_1 \sin \Phi & -\cos \varphi_1 \sin \Phi & \cos \Phi \end{bmatrix} \quad (A. 2)$$

$$[\varepsilon] = [R][E]_{Global}[R]^T = \begin{bmatrix} d\varepsilon_{xx} & d\varepsilon_{xy} & d\varepsilon_{xz} \\ sym. & d\varepsilon_{yy} & d\varepsilon_{yz} \\ sym. & sym. & d\varepsilon_{zz} \end{bmatrix} \quad (A. 3)$$

Where $[R]$ represents rotation matrix and $[\varepsilon]$ represents strain tensor in crystal coordinate system.

3- There are 12 distinguishable slip systems in the FCC structure. These are introduced in table A.1, where the hypothetical magnitude of shear strain on each slip system is denoted by a_1, a_2, \dots, d_3 . It would be possible to establish a correlation between the magnitude of shear strain on each slip system and the components of strain tensor in crystal coordinate. This is done by Eq. (A.4) through Eq. (A.9) [52].

Table A. 1- Introduction of the slip systems in the FCC crystal [52]

Plane	(111)			$(\bar{1}\bar{1}\bar{1})$			$(\bar{1}11)$			$(1\bar{1}\bar{1})$		
Dir.	01 $\bar{1}$	$\bar{1}01$	1 $\bar{1}0$	0 $\bar{1}\bar{1}$	101	$\bar{1}10$	01 $\bar{1}$	101	01 $\bar{1}$	110	$\bar{1}01$	0 $\bar{1}\bar{1}$
Mag. of shear	a_1	a_2	a_3	b_1	b_2	b_3	c_1	c_2	c_3	d_1	d_2	d_3

$$\sqrt{6d} \varepsilon_{xx} = -a_2 + a_3 - b_2 + b_3 - c_2 + c_3 - d_2 + d_3 \quad (\text{A. 4})$$

$$\sqrt{6d} \varepsilon_{yy} = +a_1 - a_3 + b_1 - b_3 - c_1 + c_3 + d_1 - d_3 \quad (\text{A. 5})$$

$$\sqrt{6d} \varepsilon_{zz} = -a_1 + a_2 - b_1 + b_2 - c_1 + c_2 - d_1 + d_2 \quad (\text{A. 6})$$

$$2\sqrt{6d} \varepsilon_{xy} = +a_1 - a_2 + b_1 - b_2 - c_1 + c_2 - d_1 + d_2 \quad (\text{A. 7})$$

$$2\sqrt{6d} \varepsilon_{xz} = -a_1 + a_3 + b_1 - b_3 + c_1 - c_3 - d_1 + d_3 \quad (\text{A. 8})$$

$$2\sqrt{6d} \varepsilon_{yz} = +a_2 - a_3 - b_2 - b_3 + c_2 - c_3 - d_2 + d_3 \quad (\text{A. 9})$$

4- For a known global state of strain and orientation of an individual grain, the left-hand sides of the set of equations A.4 to A.9 are known from step 2 (i.e. $d\varepsilon_{xx}$, $d\varepsilon_{yy}$, ...). Yet, it can be seen that the number of unknowns (i.e. a_1, a_2, \dots, d_3) is more than the number of equations; moreover, not all the equations are linearly independent. Due to the fact that $\sqrt{6d} \varepsilon_{xx} + \sqrt{6d} \varepsilon_{yy} + \sqrt{6d} \varepsilon_{zz} = 0$ from the first three equations (Eq. (A.4), Eq. (A.5), and Eq. (A.6)) only two of them are linearly independent. Therefore, for any arbitrary state of strain consisting of 5 independent strain components, at least 5 slip systems must be active for this set of equations (Eq. (A.4) to Eq. (A.9)) to have a unique answer. There are $C_5^{12} = 792$ choices of 5 slip systems from 12, and it may seem that there are 792 solutions for this system of equations, yet not all of the combinations could lead to an arbitrary shape change. This is because that the determinant of the coefficient matrix of some of these combinations is zero. For instance, consider the combination: a_1, a_2, b_1, b_2, c_1 . If one intends to calculate the magnitude of shear strains on these slip systems, one must solve the following system of linear equations written in the matrix form:

$$\begin{bmatrix} 0 & -1 & 0 & -1 & 0 \\ 1 & 0 & 1 & 0 & -1 \\ 1 & -1 & 1 & -1 & -1 \\ -1 & 0 & 1 & 0 & 1 \\ 0 & 1 & 0 & -1 & 0 \end{bmatrix} \begin{bmatrix} a_1 \\ a_2 \\ b_1 \\ b_2 \\ c_1 \end{bmatrix} = \begin{bmatrix} \sqrt{6d} \varepsilon_{xx} \\ \sqrt{6d} \varepsilon_{yy} \\ 2\sqrt{6d} \varepsilon_{xy} \\ 2\sqrt{6d} \varepsilon_{xz} \\ 2\sqrt{6d} \varepsilon_{yz} \end{bmatrix} \quad (\text{A. 10})$$

Where $d\varepsilon_{ij}$ s are not necessarily zero. It can easily be shown that the determinant of the matrix of coefficients is zero. Therefore, this combination would not result in a unique solution, and it can be interpreted that this combination of slip systems could not physically lead to an arbitrary shape change. It is shown by Taylor [4] that among 792 possible combinations, it is enough to consider only 96 of them. The general form of the system of linear equations that must be solved is:

$$\overline{A}^i \overline{\Gamma}^i = \overline{a\varepsilon} \quad (1 \leq i \leq 96) \quad (\text{A. 11})$$

In this notation \overline{A}^i is the matrix of coefficients corresponding to i th choice. $\overline{\Gamma}^i$ is an unknown vector containing 5 components of the shear strain on the chosen slip systems. $\overline{a\varepsilon}$ is the vectorized strain tensor where its components consist of the values of strain multiplied by $\sqrt{6}$ (for normal strains) or $2\sqrt{6}$ (for shear strains).

5- After solving 96 systems of linear equations, there are 96 vectors of $\overline{\Gamma}^i$ s, each corresponding to a different

choice of slip systems that would result in the prescribed shape change. Now the problem is to choose the correct answer. Based on the energy principle, among all possible actions in a system, the one that requires the least amount of energy would take place. The dissipated energy on each slip system is $\gamma\tau_{CRSS}$ where τ_{CRSS} is the critical shear stress necessary to activate that system and γ is the magnitude of the shear strain on that particular system. Taking τ_{CRSS} to be the same for all slip systems, the total required energy for each combination would be $\|\vec{\Gamma}^i\| \tau_{CRSS}$ where $\|\vec{\Gamma}^i\|$ is the first norm of the vector $\vec{\Gamma}^i$. Therefore, among all 96 solutions, the correct answer is the one with the least $\|\vec{\Gamma}^i\|$, which from now on is called $\vec{\Gamma}^*$.

6- Finally, for that individual grain in a specimen exposed to the strain state of $[E]$, the Taylor factor would be:

$$M = \frac{\|\vec{\Gamma}^*\|}{\bar{E}} = \frac{\|\vec{\Gamma}^*\|}{\bar{\epsilon}} = \frac{\bar{\sigma}}{\tau_{CRSS}} \tag{A. 12}$$

Where \bar{E} is the effective strain obtained from the global strain tensor, $\bar{\epsilon}$ is the effective strain obtained from strain tensor in crystal coordinate system, and $\bar{\sigma}$ is the effective stress. Another matter is that although combinations of more than 5 slip systems could also result in an arbitrary shape change, it is shown by Taylor [6] that any choice of combinations of more than 5 slip systems would lead to the same or more dissipated energy. As the Taylor factor of an individual grain is determined, the strength of that particular grain under the prescribed strain condition could also be determined since τ_{CRSS} is a material property and could be readily obtained by the compression test.

A. 2. Determination of the most compliant and stiff orientations

The following procedure is adopted to examine what orientation would require the least stress (most compliant orientations) and what orientation require the most stress to deform plastically (stiffest orientations). As it can be concluded from the explanations given on the strength of grain under different yielding conditions in section 2.1, the most compliant orientation would be the one for which the $M_{xx}, M_{yy}, \dots, M_{xy}$ have their minimum values. Similarly, the stiffest orientation would be the one for which the $M_{xx}, M_{yy}, \dots, M_{xy}$ have their maximum value. It may be seen in Fig. A.1 that high values of $M_{xx} + M_{yy} + M_{zz}$ correspond to low values of $M_{xy} + M_{xz} + M_{yz}$, and vice versa; therefore, it is not physically possible that an individual orientation has the maximum normal and the shear strength simultaneously. This behavior makes the problem of choosing the most compliant and stiffest orientations to the multi-

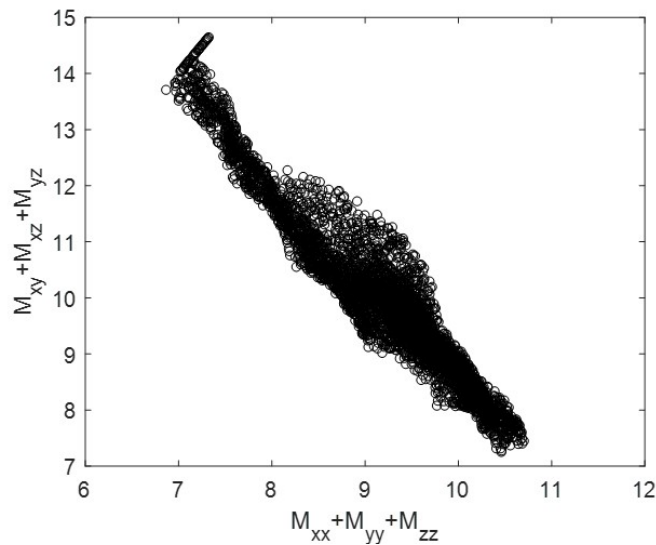


Fig. A. 1- Variation of $M_{xy} + M_{xz} + M_{yz}$ against $M_{xx} + M_{yy} + M_{zz}$ for 5000 random orientations (each circle corresponds to one random orientation).

objective optimization (MOO) problem with a non-dominated solution. It has been shown by Zadeh [53] and Goicoechea [54] that the minimum or maximum of goal function with the form of Eq. A.13 has the condition of Pareto optimality.

$$\chi = w_1 M_{xx} + w_2 M_{yy} + w_3 M_{zz} + w_4 M_{xy} + w_5 M_{xz} + w_6 M_{yz} \text{ where } \sum w_i = 1, w_i \geq 0 \quad (\text{A. 13})$$

proper choice of w_i s depends on the dominant mode of deformation in the studied forming process. For example, if large amounts of shear strain (say γ_{xy}) are imposed on the material in a particular process while other components of strain are equal to zero, the proper choice of w_i s would be $w_6=1$ with all other w_i s zero. The strain state in the microforging of miniature rods into triangular prismatic pieces is quite complicated, and the dominant strain state would probably vary as microforging proceeds. Yet some assumptions could be made: since the friction between the die walls and material are considered to be zero, $\frac{\partial u_z}{\partial x} = \frac{\partial u_y}{\partial z} = \frac{\partial u_z}{\partial y} = \frac{\partial u_y}{\partial z} = 0$ which means $\gamma_{xz} = \gamma_{yz} = 0$. In this situation, the proper choice of w_i s would be such that G^* to adopt the form of Eq. (A.14).

$$G^* = \frac{1}{4} (M_{xx} + M_{yy} + M_{zz} + M_{xy}) \quad (\text{A. 14})$$

Mathematically, optimizing G^* is analogous to optimizing G with the form of Eq. (A.15).

$$G = M_{xx} + M_{yy} + M_{zz} + M_{xy} \quad (\text{A. 15})$$

However, as M_{xx} , M_{yy} , M_{zz} and M_{xy} are intricate functions of the orientation (which may be represented by ϕ_1, Φ, ϕ_2), the analytical optimization of G is almost an impossible task to do. In such circumstances, some numerical methods might be helpful:

Assume G to be bounded between g_{min} and g_{max} , then consider $\chi_n = \{g_1, g_2, \dots, g_n\}$ to be a set consisting of the calculated values of G for n random orientations. If the maximum of χ_n is called $max(\chi_n)$ and e is defined as $e = g_{max} - max(\chi_n)$, the probability of $0 \leq e \leq \delta$ would be:

$$P(e \leq \delta) = 1 - \left(\frac{g_{max} - g_{min} - \delta}{g_{max} - g_{min}} \right)^n = 1 - \left(1 - \frac{\delta}{R} \right)^n \quad (\text{A. 16})$$

Where $R = g_{max} - g_{min}$.

Taking $\frac{\delta}{R} = 0.001$, by calculating 5000 random values for G , $P(e \leq \delta) = 99.33\%$ which means one may take $max(\chi_n)$ as g_{max} with the maximum error of $0.001R$ and 99.33% certainty, the discussion is the same for g_{min} .

In Fig. A.2, 1

pper and lower

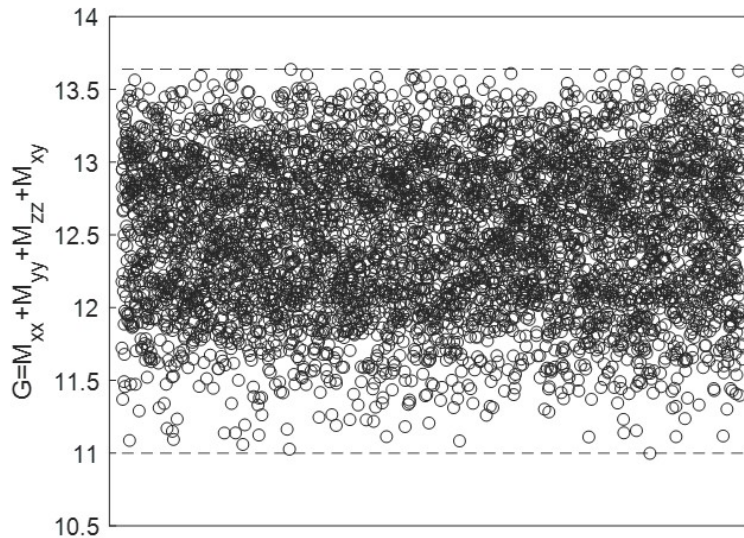


Fig. A.2 Values of $G = M_{xx} + M_{yy} + M_{zz} + M_{xy}$ for 5000 random orientations (each circle corresponds to one random orientation)

limits are possible choices for the stiffest and the most compliant orientations.

A. 3. The implication of combined Hill-Taylor theory in ABAQUS

To implement Hill's yield criterion in ABAQUS software, according to the ABAQUS user's manual, six parameters must be defined:

$$R_{11} = \bar{\sigma}_{11} / \sigma^0, \quad R_{22} = \bar{\sigma}_{22} / \sigma^0, \quad R_{33} = \bar{\sigma}_{33} / \sigma^0, \quad R_{12} = \bar{\sigma}_{12} / \tau^0, \quad R_{13} = \bar{\sigma}_{13} / \tau^0, \quad R_{23} = \bar{\sigma}_{23} / \tau^0$$

Where, for example, $\bar{\sigma}_{11}$ is the normal stress in 1-direction that causes yielding if only the force is applied in the sense of 1- direction, and $\bar{\sigma}_{23}$ is the shear stress that causes yielding if only the force is applied to the plane perpendicular to the 2- direction in the sense of 3- direction; σ^0 and $\tau^0 = \sigma^0 / \sqrt{3}$ are also reference normal and shear strength that the user enters as material property. Based on the combined Hill-Taylor model, one may express the normal strength of grain in 1-direction as $\bar{\sigma}_{11} = M_{11} \tau_{CRSS}$, therefore, if one takes σ^0 as τ_{CRSS} for the reference strength, then R_{11} can be taken to be equal to M_{11} . Similarly, $\bar{\sigma}_{23}$ can be expressed as $\bar{\sigma}_{23} = M_{23} \tau_{CRSS} / \sqrt{3}$, and since $\tau^0 = \sigma^0 / \sqrt{3} = \tau_{CRSS} / \sqrt{3}$; therefore, R_{23} can be taken to be equal to M_{23} . Based on the foregoing discussion, to execute the combined Hill-Taylor model, τ_{CRSS} and its dependence on γ must be entered as the plastic properties of the material, and M_{ij} s must be entered as R_{ij} s. In order to implement Hill's plasticity model in Abaqus, it is necessary to define a coordinate system named material orientation. Based on the procedure adopted to calculate M_{ij} s and by looking at Eq. (A.12), it can be seen that M_{ij} s inherently correlate the material coordinate system to the global coordinate system. Therefore, during the implementation of this model in Abaqus, it is not necessary to define a specific material orientation for each grain, and it can be taken as the global coordinate system for all grains.